# A SCALABLE LAPLACE APPROXIMATION FOR NEURAL NETWORKS

**Anonymous authors**
Paper under double-blind review

## ABSTRACT

We leverage recent insights from second-order optimisation for neural networks to construct a Kronecker factored Laplace approximation to the posterior over the weights of a trained network. Our approximation requires no modification of the training procedure, enabling practitioners to estimate the uncertainty of their models currently used in production without having to retrain them. We extensively compare our method to using Dropout and a diagonal Laplace approximation for estimating the uncertainty of a network. We demonstrate that our Kronecker factored method leads to better uncertainty estimates on out-of-distribution data and is more robust to simple adversarial attacks. Our approach only requires calculating two square curvature factor matrices for each layer. Their size is equal to the respective square of the input and output size of the layer, making the method efficient both computationally and in terms of memory usage. We illustrate its scalability by applying it to a state-of-the-art convolutional network architecture.

## 1 INTRODUCTION

Neural networks are most commonly trained in a maximum likelihood/MAP setting, which only yields point estimates of the parameters, ignoring any uncertainty about them. This often leads to overconfident predictions, especially in regimes that are weakly covered by training data or far away from the data manifold. While the confidence of wrong predictions is usually irrelevant in a research context, it is essential that a Machine Learning algorithm knows when it does not know in the real world, as the consequences of mistakes can be fatal, be it when driving a car or diagnosing a disease.

The Bayesian framework of statistics provides a principled way for avoiding overconfidence in the parameters by treating them as unknown quantities and integrating over all possible values. Specifically, for the prediction of new data under a model, it fits a posterior distribution over the parameters given the training data and weighs the contribution of each setting of the parameters to the prediction by the probability of the data under those parameters times their prior probability. However, the posterior of neural networks is usually intractable due to their size and nonlinearity.

There has been previous interest in integrating neural networks into the Bayesian framework (MacKay, 1992; Hinton & Van Camp, 1993; Neal, 1993; Barber & Bishop, 1998), however these approaches were designed for small networks by current standards. Recent adaptations to architectures of modern scale rely on crude approximations of the posterior to become tractable. All of (Graves, 2011; Hernández-Lobato & Adams, 2015; Blundell et al., 2015) assume independence between the individual weights. While they achieve good results on small datasets, this strong restriction of the posterior is susceptible to underestimating the uncertainty, in particular when minimising the KL-objective. The approach in (Gal & Ghahramani, 2016) requires the use of certain stochastic regularisers which are not commonly present in most recent architectures. Furthermore, it is not clear if the approximate posterior defined by these regularisers is a good fit to the true posterior.

Recent work on second-order optimisation of neural networks (Martens & Grosse, 2015; Botev et al., 2017) has demonstrated that the diagonal blocks of the curvature can be well approximated by a Kronecker product. We combine this insight with the idea of modelling the posterior over the weights as a Gaussian, using a Laplace approximation (MacKay, 1992) with Kronecker factored covariance matrices. This leads to a computationally efficient *matrix* normal posterior distribution (Gupta & Nagar, 1999) over the weights of every layer. Since the Laplace approximation is applied after training, our approach can be used to obtain uncertainty estimates from existing networks.

## 2 THE CURVATURE OF NEURAL NETWORKS

Our method is inspired by recent Kronecker factored approximations of the curvature of a neural network (Martens & Grosse, 2015; Botev et al., 2017) for optimisation and we give a high-level review of these in the following. While the two methods approximate the Gauss-Newton and Fisher matrix respectively, we base all of our discussion on the Hessian in order to be as general as possible. It is usually necessary to use the Gauss-Newton or Fisher instead, as they are guaranteed to be p.s.d.

### 2.1 NEURAL NETWORK NOTATION

We denote a feedforward network as taking an input $a_0 = x$ and producing an output $h_L$. The intermediate representations for layers $\lambda = 1, ..., L$ are denoted as $h_\lambda = W_\lambda a_{\lambda-1}$ and $a_\lambda = f_\lambda(h_\lambda)$. We refer to $a_\lambda$ as the activations, and $h_\lambda$ as the (linear) pre-activations. The bias terms are absorbed into the $W_\lambda$ by appending a 1 to each $a_\lambda$. The network parameters are optimised w.r.t. an error function $E(y, h_L)$ for targets $y$. Most commonly used error functions, such as squared error and categorical cross-entropy, can be interpreted as exponential family negative log likelihoods $-\log p(y|h_L)$.

### 2.2 KRONECKER FACTORED SECOND-ORDER OPTIMISATION

Traditional second-order methods use either the Hessian matrix or a positive semi-definite approximation thereof to generate parameter updates of the form $\Delta = C^{-1}g$, where $C$ is the chosen curvature matrix and $g$ the gradient of the error function parameterised by the network. However, this curvature matrix is infeasbile to compute for modern neural networks as their number of parameters is often in the millions, rendering the size of $C$ of the order of several terabytes.

Recent work (Martens & Grosse, 2015; Botev et al., 2017) exploits that, for *a single data point*, the diagonal blocks of these curvature matrices are Kronecker factored:

$$H_\lambda = \frac{\partial^2 E}{\partial \operatorname{vec}(W_\lambda) \partial \operatorname{vec}(W_\lambda)} = \mathcal{Q}_\lambda \otimes \mathcal{H}_\lambda \tag{1}$$

where $H_\lambda$ is the Hessian w.r.t. the weights in layer $\lambda$. $\mathcal{Q}_\lambda = a_{\lambda-1} a_{\lambda-1}^\mathsf{T}$ denotes the covariance of the incoming activations $a_{\lambda-1}$ and $\mathcal{H}_\lambda = \frac{\partial^2 E}{\partial h_\lambda \partial h_\lambda}$ the pre-activation Hessian, i.e. the Hessian of the error w.r.t. the linear pre-activations $h_\lambda$ in a layer. We provide the derivation for this result as well as the recursion for calculating $\mathcal{H}$ in Appendix A.

The Kronecker factorisation holds two key advantages: the matrices that need be computed and stored are much smaller — if we assume all layers to be of dimensionality $D$, the two factors are each of size $D^2$, whereas the full Hessian for the weights of only one layer would have $D^4$ elements. Furthermore, the inverse of a Kronecker product is equal to the Kronecker product of the inverses, so it is only necessary to invert those two moderately sized matrices.

In order to maintain this structure over a minibatch of data, all Kronecker factored second-order methods make two core approximations: First, they only model the diagonal blocks corresponding to the weights of a layer, such that the curvature decomposes into $L$ independent matrices. Second, they assume $\mathcal{Q}_\lambda$ and $\mathcal{H}_\lambda$ to be independent. This is in order to maintain the Kronecker factorisation in expectation, i.e. $\mathbb{E}\left[\mathcal{Q}_\lambda \otimes \mathcal{H}_\lambda\right] \approx \mathbb{E}\left[\mathcal{Q}_\lambda\right] \otimes \mathbb{E}\left[\mathcal{H}_\lambda\right]$, since the expectation of a Kronecker product is not guaranteed to be Kronecker factored itself.

The main difference between the Kronecker factored second-order optimisers lies in how they efficiently approximate $\mathbb{E}\left[\mathcal{H}_\lambda\right]$. For exact calculation, it would be necessary to pass back an entire matrix per data point in a minibatch, which imposes infeasible memory and computational requirements. KFRA (Botev et al., 2017) simply passes back the expectation at every layer, while KFAC (Martens & Grosse, 2015) utilises the Fisher identity to only propagate a vector rather than a matrix, approximating the Kronecker factors with a stochastic rank-one matrix for each data point. The diagonal blocks of the Hessian and Gauss-Newton matrix are equal for neural networks with piecewise linear activation functions (Botev et al., 2017), thus both methods can be used to directly approximate the diagonal blocks of the Hessian of such networks, as the Gauss-Newton and Fisher are equivalent for networks that parameterise an exponential family log likelihood.

# 3 A SCALABLE LAPLACE APPROXIMATION FOR NEURAL NETWORKS

## 3.1 THE LAPLACE APPROXIMATION

The standard Laplace approximation is obtained by taking the second-order Taylor expansion around a mode of a distribution. For a neural network, such a mode can be found using standard gradient-based methods. Specifically, if we approximate the negative log posterior over the weights of a network given some data $\mathcal{D}$ around a MAP estimate $\theta^*$, we obtain:

$$-\log p(\theta|\mathcal{D}) \approx -\log p(\theta^*|\mathcal{D}) - \frac{1}{2}(\theta - \theta^*)^\intercal \bar{H}(\theta - \theta^*) \tag{2}$$

where $\theta = [\mathrm{vec}(W_1), ..., \mathrm{vec}(W_L)]$ is the stacked vector of weights and $\bar{H} = \mathbb{E}\left[H\right]$ the average Hessian of the negative log posterior[1]. The first order term is missing because we expand the function around a maximum $\theta^*$, where the gradient is zero. If we exponentiate this equation, it is easy to notice that the right-hand side is of Gaussian functional form for $\theta$, thus we obtain a normal distribution by integrating over it. The posterior over the weights is then approximated as Gaussian:

$$\theta \sim \mathcal{N}(\theta^*, \bar{H}^{-1}) \tag{3}$$

assuming $\bar{H}$ is p.s.d. We can then approximate the posterior mean when predicting on unseen data $D^*$ by averaging the predictions of $T$ Monte Carlo samples $\theta^{(t)}$ from the approximate posterior:

$$p(\mathcal{D}^*|\mathcal{D}) = \int p(\mathcal{D}^*|\theta)p(\theta|\mathcal{D})d\theta \approx \frac{1}{T}\sum_{t=1}^{T} p(\mathcal{D}^*|\theta^{(t)}) \tag{4}$$

## 3.2 DIAGONAL LAPLACE APPROXIMATION

Unfortunately, it is not feasible to compute or invert the Hessian matrix w.r.t. all of the weights jointly. An approximation that is easy to compute in modern automatic differentiation frameworks is the diagonal of the Fisher matrix $F$, which is simply the expectation of the squared gradients:

$$H \approx \mathrm{diag}(F) = \mathrm{diag}(\mathbb{E}\left[\nabla_\theta \log p(y|x) \nabla_\theta \log p(y|x)^\intercal\right]) = \mathrm{diag}(\mathbb{E}\left[(\nabla_\theta \log p(y|x))^2\right]) \tag{5}$$

where $\mathrm{diag}$ extracts the diagonal of a matrix or turns a vector into a diagonal matrix. Such diagonal approximations to the curvature of a neural network have been used successfully for pruning the weights (LeCun et al., 1990) and, more recently, for transfer learning (Kirkpatrick et al., 2017).

This corresponds to modelling the weights with a Normal distribution with diagonal covariance:

$$\mathrm{vec}(W_\lambda) \sim \mathcal{N}(\mathrm{vec}(W_\lambda^*), \mathrm{diag}(F_\lambda)^{-1}) \quad \text{for } \lambda = 1, \ldots, L \tag{6}$$

Unfortunately, even if the second-order Taylor approximation is accurate, this will place significant probability mass in low probability areas of the true posterior if some weights exhibit high covariance. This can be seen for a highly correlated two-dimensional Gaussian that only allows the value of one dimension to be highly positive when the other one is highly negative. A diagonal approximation of such a Gaussian would allow the two values to also be jointly positive or negative.

## 3.3 KRONECKER FACTORED LAPLACE APPROXIMATION

So while it is desirable to model the covariance between the weights, some approximations are needed in order to remain computationally efficient. First, we assume the weights of the different layers to be independent. This corresponds to the block-diagonal approximation in KFAC and

[1] The average Hessian is typically scaled by the number of data points $N$. In order to keep the notation uncluttered, we develop our basic methods in terms of the average Hessian and discuss the scaling separately.

KFRA, which empirically preserves sufficient information about the curvature to obtain competitive optimisation performance. For our purposes this means that our posterior factorises over the layers.

As discussed above, the Hessian of the log-likelihood for a single datapoint is Kronecker factored, and we denote the two factor matrices as $H_\lambda = \mathcal{Q}_\lambda \otimes \mathcal{H}_\lambda$.[2] By further assuming independence between $\mathcal{Q}$ and $\mathcal{H}$ in all layers, we can approximate the expected Hessian of each layer as:

$$\mathbb{E}\left[H_\lambda\right] = \mathbb{E}\left[\mathcal{Q}_\lambda \otimes \mathcal{H}_\lambda\right] \approx \mathbb{E}\left[\mathcal{Q}_\lambda\right] \otimes \mathbb{E}\left[\mathcal{H}_\lambda\right] \tag{7}$$

Hence, the Hessian of every layer is Kronecker factored over an *entire dataset* and the Laplace approximation can be approximated by a product of Gaussians. Each Gaussian has a Kronecker factored covariance, corresponding to a *matrix* normal distribution (Gupta & Nagar, 1999), which considers the two Kronecker factors of the covariance to be the covariances of the rows and columns of a matrix. The two factors are much smaller than the full covariance and allow for significantly more efficient inversion and sampling (we review the matrix normal distribution in Appendix B).

Our resulting posterior for the weights in layer $\lambda$ is then:

$$W_\lambda \sim \mathcal{MN}(W_\lambda^*, \bar{\mathcal{Q}}_\lambda^{-1}, \bar{\mathcal{H}}_\lambda^{-1}) \tag{8}$$

In contrast to optimisation methods, we do not need to approximate $\mathbb{E}\left[\mathcal{H}_\lambda\right]$ as it is only calculated once. However, when it is possible to augment the data (e.g. randomised cropping of images), it may be advantageous. We provide a more detailed discussion of this in Appendix C.

### 3.4 Incorporating the Prior and Regularising the Curvature Factors

Just as the log posterior, the Hessian decomposes into a term depending on the data log likelihood and one on the prior. For the commonly used $L_2$-regularisation, corresponding to a Gaussian prior, the Hessian is equal to the precision of the prior times the identity matrix. We approximate this by adding a multiple of the identity to each of the Kronecker factors from the log likelihood:

$$H_\lambda = N\,\mathbb{E}\left[-\frac{\partial^2 \log p(\mathcal{D}|\theta)}{\partial \theta^2}\right] + \tau I \approx (\sqrt{N}\,\mathbb{E}\left[\mathcal{Q}_\lambda\right] + \sqrt{\tau} I) \otimes (\sqrt{N}\,\mathbb{E}\left[\mathcal{H}_\lambda\right] + \sqrt{\tau} I) \tag{9}$$

where $\tau$ is the precision of the Gaussian prior on the weights and $N$ the size of the dataset. However, we can also treat them as hyperparameters and optimise them w.r.t. the predictive performance on a validation set. We emphasise that this can be done without retraining the network, so it does not impose a large computational overhead and is trivial to parallelise.

Setting $N$ to a larger value than the size of the dataset can be interpreted as including duplicates of the data points as pseudo-observations. Adding a multiple of the uncertainty to the precision matrix decreases the uncertainty about each parameter. This has a regularising effect both on our approximation to the true Laplace, which may be overestimating the variance in certain directions due to ignoring the covariances between the layers, as well as the Laplace approximation itself, which may be placing probability mass in low probability areas of the true posterior.

## 4 Related Work

Most recent attempts to approximating the posterior of a neural network are based on formulating an approximate distribution to the posterior and optimising the variational lower bound w.r.t. its parameters. (Graves, 2011; Blundell et al., 2015; Kingma et al., 2015) as well as the EP-based approaches of (Hernández-Lobato & Adams, 2015) and (Ghosh et al., 2016) assume independence between the individual weights which, particularly when optimising the KL divergence, often lets the model underestimate the uncertainty about the weights. Gal & Ghahramani (2016) interpret Dropout to approximate the posterior with a mixture of delta functions, assuming independence

[2] We assume a uniform prior for now, such that the Hessians of the posterior and the log likelihood are equal. We discuss how we incorporate a non-zero Hessian of a prior into the Kronecker factors in the next section.

between the columns. (Lakshminarayanan et al., 2016) suggest using an ensemble of networks for estimating the uncertainty.

Our work is a scalable approximation of (MacKay, 1992). Since the per-layer Hessian of a neural network is infeasible to compute, we suggest a factorisation of the covariance into a Kronecker product, leading to a more efficient *matrix* normal distribution. The posterior that we obtain is reminiscent of (Louizos & Welling, 2016) and (Sun et al., 2017), who optimise the parameters of a matrix normal distribution as their weights, which requires a modification of the training procedure.

Our method is not necessarily orthogonal to existing approaches. In particular, it could be combined with Dropout by sampling a fixed number of masks, optimising the resulting networks to convergence and then applying the Kronecker factored Laplace approximation to each of them, leading to an approximation of the posterior with a mixture of Gaussians.

## 5 Experiments

Since the Laplace approximation is a method for *predicting* in a Bayesian manner and not for training, we focus on comparing to uncertainty estimates obtained from Dropout (Gal & Ghahramani, 2016). The trained networks will be identical, but the prediction methods will differ. We also compare to a diagonal Laplace approximation to highlight the benefit from modelling the covariances between the weights. All experiments are implemented using Theano (Theano Development Team, 2016) and Lasagne (Dieleman et al., 2015). The code will be made available upon publication.

### 5.1 Toy Regression Dataset

As a first experiment, we visualise the uncertainty obtained from the two Laplace approximations on a toy regression dataset, similar to (Hernández-Lobato & Adams, 2015). For this we create a dataset of 20 uniformly distributed points $x \sim \mathcal{U}(-4, 4)$ and sample $y \sim \mathcal{N}(x^3, 3^2)$. In contrast to (Hernández-Lobato & Adams, 2015), we use a two-layer network with seven units per layer rather than one layer with 100 units. This is because both the input and output are one-dimensional, hence the weight matrices are vectors and the matrix normal distribution reduces to a common multivariate normal distribution. Furthermore, the Laplace approximation is sensitive to the number of the data points relative to the number of parameters. In comparison to Hernández-Lobato & Adams (2015)'s network, ours has 78 instead of 301 parameters and our Kronecker factored Laplace approximation estimates 132 curvature directions. The main reason for this reduction in model size is that we want to visualise the effect of our approximation without any regularisation.

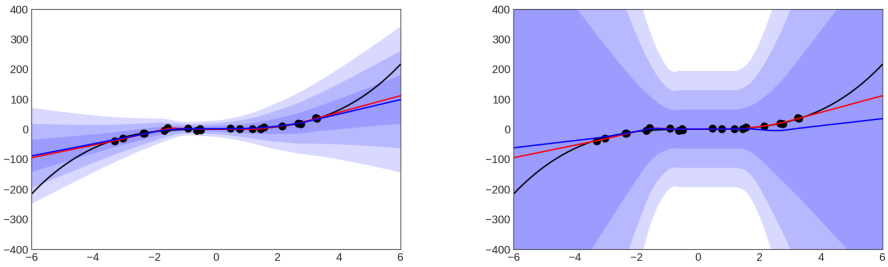


(a) Kronecker factored Laplace Approximation (b) Diagonal Laplace Approximation

Figure 1: Toy regression uncertainty. Black dots are data points, the black line shows the underlying noiseless function. The red line shows the deterministic prediction of the trained network, the blue line the mean output of 250 samples. Each shade of blue visualises one additional standard deviation.

Fig. 1 shows the uncertainty obtained from the Kronecker factored and the diagonal Laplace approximation on the same network trained on the toy dataset. Both approximations are increasingly uncertain away from the data, as the true posterior estimated from HMC samples (see (Hernández-Lobato & Adams, 2015) for figures for their model). However, the diagonal approximation vastly overestimates the uncertainty even close to the data, as it ignores the covariance between the weights.

### 5.2 OUT-OF-DISTRIBUTION UNCERTAINTY

For a more realistic test, similar to (Louizos & Welling, 2017), we assess the uncertainty of the predictions when classifying data from a different distribution than the training data. For this we train a network with two layers of $1024$ hidden units and ReLU transfer functions to classify MNIST digits. We use a learning rate of $10^{-2}$ and momentum of $0.9$ for $250$ epochs. We apply Dropout with $p$=$0.5$ after each inner layer, as our chief interest is to compare against its uncertainty estimates. We further use $L_2$-regularisation with a factor of $10^{-2}$ and randomly binarise the images during training according to their pixel intensities and draw $1,000$ such samples per datapoint for estimating the curvature factors. We use this network to classify the images in the notMNIST dataset[3], which contains $28\times28$ grey-scale images of the letters 'A' to 'J' from various computer fonts, i.e. not digits. An ideal classifier would make uniform predictions over its classes.

We compare the uncertainty obtained by predicting the digit class of the notMNIST images using 1. a deterministic forward pass through the Dropout trained network, 2. by sampling different Dropout masks and averaging the predictions, and by sampling different weight matrices from 3. the matrix normal distribution obtained from our Kronecker factored Laplace approximation as well as 4. the diagonal one. We use $100$ samples for the stochastic forward passes and optimise the hyperparameters of the Laplace approximations w.r.t. the cross-entropy on the validation set of MNIST.

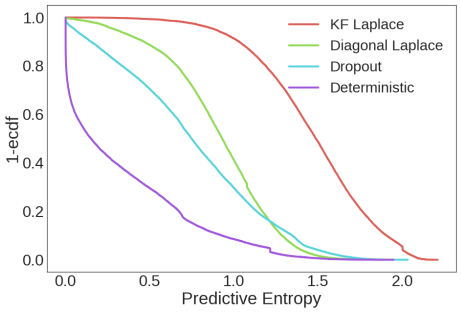


Figure 2: Predictive entropy on notMNIST obtained from different methods for the forward pass on a network trained on MNIST.

We measure the uncertainty of the different methods as the entropy of the predictive distribution, which has a minimal value of $0$ when a single class is predicted with probability $1$ and a maximum of about $2.3$ when all classes are predicted uniformly. Fig. 2 shows the inverse empirical cumulative distribution of the entropy values obtained from the four methods. Consistent with the results in (Gal & Ghahramani, 2016), averaging the probabilities of multiple passes through the network yields predictions with higher uncertainty than a deterministic pass that approximates the geometric average (Srivastava et al., 2014). However, there still are some images that are predicted to be a digit with certainty. Our Kronecker factored Laplace approximation makes hardly any predictions with absolute certainty and assigns high uncertainty to most of the letters as desired. The diagonal Laplace approximation required stronger regularisation towards predicting deterministically, yet it performs similarly to Dropout.

One might suspect, that this increased uncertainty comes at the cost of a reduced classification performance. After all, a classifier that always predicts a uniform distribution over its classes would attain perfect uncertainty on out-of-sample data. As shown in Table 1 in the appendix, however, the network makes predictions on the test set of MNIST with similar accuracy to the deterministic forward pass and MC Dropout when using our approximation.

### 5.3 ADVERSARIAL EXAMPLES

To further test the robustness of our prediction method close to the data distribution, we perform an adversarial attack on a neural network. As first demonstrated in (Szegedy et al., 2013), neural networks are prone to being fooled by gradient-based changes to their inputs. Li & Gal (2017) suggest, and provide empirical support, that Bayesian models may be more robust to such attacks, since they implicitly form an infinitely large ensemble by integrating over the model parameters. For our experiments, we use the fully connected net trained on MNIST from the previous section and compare the sensitivity of the different prediction methods for two kinds of adversarial attacks.

[3]From: `http://yaroslavvb.blogspot.nl/2011/09/notmnist-dataset.html`

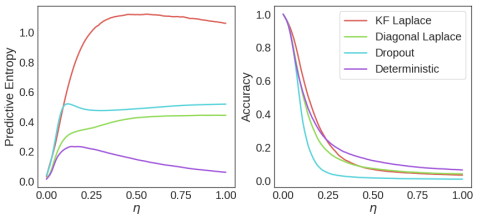


Figure 3: Untargeted adversarial attack.

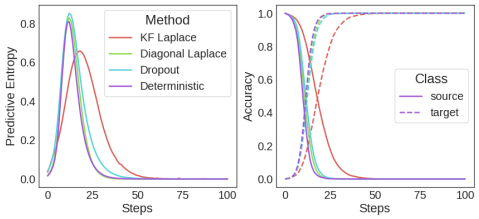


Figure 4: Targeted adversarial attack.

First, we use the untargeted Fast Gradient Sign method $x_{adv} = x - \eta \operatorname{sgn}(\nabla_x \max_y \log p^{(M)}(y|x))$ suggested in (Goodfellow et al., 2014), which takes the gradient of the class predicted with maximal probability by method $M$ w.r.t. the input $x$ and reduces this probability with varying step size $\eta$. This step size is rescaled by the difference between the maximal and minimal value per dimension in the dataset. It is to be expected that this method generates examples away from the data manifold, as there is no clear subset of the data that corresponds to e.g. "not ones".

Fig. 3 shows the average predictive uncertainty and the accuracy on the original class on the MNIST test set as the step size $\eta$ increases. The Kronecker factored Laplace approximation achieves significantly higher uncertainty than any other prediction method as the images move away from the data. Both the diagonal and the Kronecker factored Laplace maintain higher accuracy than MC Dropout on their original predictions. Interestingly, the deterministic forward pass appears to be most robust in terms of accuracy, however it has much smaller uncertainty on the predictions it makes and will confidently predict a false class for most images, whereas the other methods are more uncertain.

Furthermore, we perform a targeted attack that attempts to force the network to predict a specific class, in our case '0' following (Li & Gal, 2017). Hence, for each method, we exclude all data points in the test set that are already predicted as '0'. The updates are of similar form to the untargeted attack, however they increase the probability of the pre-specified class $y$ rather than decreasing the current maximum as $x_y^{(t+1)} = x_y^{(t)} + \eta \operatorname{sgn}(\nabla_x \log p^{(M)}(y|x_y^{(t)}))$, where $x_y^{(0)} = x$.

We use a step size of $\eta{=}10^{-2}$ for the targeted attack. The uncertainty and accuracy on the original and target class are shown in Fig. 4. Here, the Kronecker factored Laplace approximation has slightly smaller uncertainty at its peak in comparison to the other methods, however it appears to be much more robust. It only misclassifies over $50\%$ of the images after about $20$ steps, whereas for the other methods this is the case after roughly $10$ steps and reaches $100\%$ accuracy on the target class after almost $50$ updates, whereas the other methods are fooled on all images after about $25$ steps.

In conjunction with the experiment on notMNIST, it appears that the Laplace approximation achieves higher uncertainty than Dropout away from the data, as in the untargeted attack. In the targeted attack it exhibits smaller uncertainty than Dropout, yet it is more robust to having its prediction changed. The diagonal Laplace approximation again performs similarly to Dropout.

### 5.4 Uncertainty on Misclassifications

To highlight the scalability of our method, we apply it to a state-of-the-art convolutional network architecture. Recently, deep residual networks (He et al., 2016a;b) have been the most successful ones among those. As demonstrated in (Grosse & Martens, 2016), Kronecker factored curvature methods are applicable to convolutional layers by interpreting them as matrix-matrix multiplications.

We compare our uncertainty estimates on wide residual networks (Zagoruyko & Komodakis, 2016), a recent variation that achieved competitive performance on CIFAR100 (Krizhevsky & Hinton, 2009) while, in contrast to most other residual architectures, including Dropout at specific points. While this does not correspond to using Dropout in the Bayesian sense (Gal & Ghahramani, 2015), it allows us to at least compare our method to the uncertainty estimates obtained from Dropout.

We note that it is straightforward to incorporate batch normalisation (Ioffe & Szegedy, 2015) into the curvature backpropagation algorithms, so we apply a standard Laplace approximation to its parameters as well. We are not aware of any interpretation of Dropout as performing Bayesian inference on the parameters of batch normalisation. Further implementation details are in Appendix F.

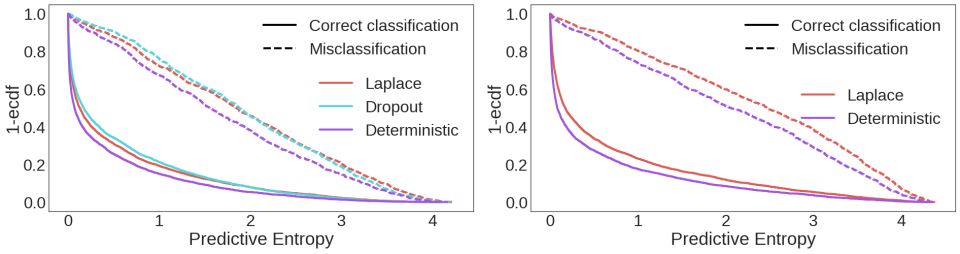


(a) Dropout Wide Resnet

(b) Deterministic Wide Resnet

Figure 5: Inverse ecdf of the predictive entropy from Wide Residual Networks trained with and without Dropout on CIFAR100. For misclassifications, curves on top corresponding to higher uncertainty are desirable, and curves on the bottom for correct classifications.

Again, the accuracy of the prediction methods is comparable (see Table 2 in Appendix E). For calculating the curvature factors, we draw $5,000$ samples per image using the same data augmentation as during training, effectively increasing the dataset size to $2.5 \times 10^8$. The diagonal approximation had to be regularised to the extent of becoming deterministic, so we omit it from the results.

In Fig. 5 we compare the distribution of the predictive uncertainty on the test set[4]. We distinguish between the uncertainty on correct and incorrect classifications, as the mistakes of a system used in practice may be less severe if the network can at least indicate that it is uncertain. Thus, high uncertainty on misclassifications and low uncertainty on correct ones would be desirable, such that a system could return control to a human expert when it can not make a confident decision. In general, the network tends to be more uncertain on its misclassifcations than its correct ones regardless of whether it was trained with or without Dropout and of the method used for prediction. Both Dropout and the Laplace approximation similarly increase the uncertainty in the predictions, however this is irrespective of the correctness of the classification. Yet, our experiments show that the Kronecker factored Laplace approximation can be scaled to modern convolutional networks and maintain good classification accuracy while having similar uncertainty about the predictions as Dropout.

We had to use much stronger regularisation for the Laplace approximation on the wide residual network, possibly because the block-diagonal approximation becomes more inaccurate on deep networks, possibly because the number of parameters is much higher relative to the number of data. It would be interesting to see how the Laplace approximations behaves on a much larger dataset like ImageNet for similarly sized networks, where we have a better ratio of data to parameters and curvature directions. However, even on a relatively small dataset like CIFAR we did not have to regularise the Laplace approximation to the degree of the posterior becoming deterministic.

## 6 Conclusion

We presented a scalable approximation to the Laplace approximation for the posterior of a neural network and provided experimental results suggesting that the uncertainty estimates are on par with current alternatives like Dropout, if not better. It enables practitioners to obtain principled uncertainty estimates from their models, even if they were trained in a maximum likelihood/MAP setting.

There are many possible extensions to this work. One would be to automatically determine the scale and regularisation hyperparameters of the Kronecker factored Laplace approximation using the model evidence similar to how (MacKay, 1992) interpolates between the data log likelihood and the width of the prior. A challenging application would be active learning, where only little data is available relative to the number of curvature directions that need to be estimated. Furthermore, our Laplace approximation could be combined with Dropout to obtain a Gaussian mixture posterior over the weights, which would result in a more flexible approximate posterior.

[4]We use the first $5,000$ images as a validation set to tune the hyperparameters of our Laplace approximation and the final $5,000$ ones for evaluating the predictive uncertainty on all methods.

## REFERENCES


Anoop Korattikara Balan, Vivek Rathod, Kevin P Murphy, and Max Welling. Bayesian Dark Knowledge. In *Advances in Neural Information Processing Systems*, pp. 3438–3446, 2015.

David Barber and Christopher M Bishop. Ensemble Learning for Multi-layer Networks. In *Advances in Neural Information Processing Systems*, pp. 395–401, 1998.

Charles Blundell, Julien Cornebise, Koray Kavukcuoglu, and Daan Wierstra. Weight Uncertainty in Neural Networks. In *ICML*, pp. 1613–1622, 2015.

Aleksandar Botev, Hippolyt Ritter, and David Barber. Practical Gauss-Newton Optimisation for Deep Learning. In *ICML*, pp. 557 – 565, 2017.

Sander Dieleman, Jan Schlüter, Colin Raffel, Eben Olson, Søren Kaae Sønderby, Daniel Nouri, et al. Lasagne: First release., August 2015.

Yarin Gal and Zoubin Ghahramani. Bayesian Convolutional Neural Networks with BernoulliAapproximate Variational Inference. *arXiv preprint arXiv:1506.02158*, 2015.

Yarin Gal and Zoubin Ghahramani. Dropout as a Bayesian Approximation: Representing Model Uncertainty in Deep Learning. In *ICML*, pp. 1050–1059, 2016.

Soumya Ghosh, Francesco Maria Delle Fave, and Jonathan S Yedidia. Assumed Density Filtering Methods for Learning Bayesian Neural Networks. In *AAAI*, pp. 1589–1595, 2016.

Ian J Goodfellow, Jonathon Shlens, and Christian Szegedy. Explaining and Harnessing Adversarial Examples. *arXiv preprint arXiv:1412.6572*, 2014.

Alex Graves. Practical Variational Inference for Neural Networks. In *Advances in Neural Information Processing Systems*, pp. 2348–2356, 2011.

Roger Grosse and James Martens. A Kronecker-factored Approximate Fisher Matrix for Convolution Layers. In *ICML*, pp. 573–582, 2016.

Arjun K Gupta and Daya K Nagar. *Matrix Variate Distributions*, volume 104. CRC Press, 1999.

Kaiming He, Xiangyu Zhang, Shaoqing Ren, and Jian Sun. Deep Residual Learning for Image Recognition. In *Proceedings of the IEEE conference on computer vision and pattern recognition*, pp. 770–778, 2016a.

Kaiming He, Xiangyu Zhang, Shaoqing Ren, and Jian Sun. Identity Mappings in Deep Residual Networks. In *European Conference on Computer Vision*, pp. 630–645. Springer, 2016b.

José Miguel Hernández-Lobato and Ryan Adams. Probabilistic Backpropagation for Scalable Learning of Bayesian Neural Networks. In *ICML*, pp. 1861–1869, 2015.

Geoffrey E Hinton and Drew Van Camp. Keeping the Neural Networks Simple by Minimizing the Description Length of the Weights. In *COLT*, pp. 5–13, 1993.

Sergey Ioffe and Christian Szegedy. Batch Normalization: Accelerating Deep Network Training by Reducing Internal Covariate Shift. In *ICML*, pp. 448–456, 2015.

Diederik P Kingma, Tim Salimans, and Max Welling. Variational Dropout and the Local Reparameterization Trick. In *Advances in Neural Information Processing Systems*, pp. 2575–2583, 2015.

James Kirkpatrick, Razvan Pascanu, Neil Rabinowitz, Joel Veness, Guillaume Desjardins, Andrei A Rusu, Kieran Milan, John Quan, Tiago Ramalho, Agnieszka Grabska-Barwinska, et al. Overcoming Catastrophic Forgetting in Neural Networks. *Proceedings of the National Academy of Sciences*, pp. 201611835, 2017.

Alex Krizhevsky and Geoffrey Hinton. Learning Multiple Layers of Features from Tiny Images. 2009.

Balaji Lakshminarayanan, Alexander Pritzel, and Charles Blundell. Simple and Scalable Predictive Uncertainty Estimation using Deep Ensembles. *arXiv preprint arXiv:1612.01474*, 2016.

Yann LeCun, John S. Denker, and Sara A. Solla. Optimal Brain Damage. In *Advances in Neural Information Processing Systems*, pp. 598–605, 1990.

Yingzhen Li and Yarin Gal. Dropout Inference in Bayesian Neural Networks with Alpha-divergences. *arXiv preprint arXiv:1703.02914*, 2017.

Christos Louizos and Max Welling. Structured and Efficient Variational Deep Learning with Matrix Gaussian Posteriors. In *ICML*, pp. 1708–1716, 2016.

Christos Louizos and Max Welling. Multiplicative Normalizing Flows for Variational Bayesian Neural Networks. In *ICML*, pp. 2218–2227, 2017.

David J. C. MacKay. A Practical Bayesian Framework for Backpropagation Networks. *Neural Computation*, 4(3):448–472, 1992.

James Martens and Roger Grosse. Optimizing Neural Networks with Kronecker-factored Approximate Curvature. In *ICML*, pp. 2408–2417, 2015.

Radford M Neal. Bayesian Learning via Stochastic Dynamics. In *Advances in Neural Information Processing Systems*, pp. 475–482, 1993.

Nitish Srivastava, Geoffrey E Hinton, Alex Krizhevsky, Ilya Sutskever, and Ruslan Salakhutdinov. Dropout: A Simple Way to Prevent Neural Networks from Overfitting. *Journal of Machine Learning Research*, 15(1):1929–1958, 2014.

Shengyang Sun, Changyou Chen, and Lawrence Carin. Learning Structured Weight Uncertainty in Bayesian Neural Networks. In *Artificial Intelligence and Statistics*, pp. 1283–1292, 2017.

Christian Szegedy, Wojciech Zaremba, Ilya Sutskever, Joan Bruna, Dumitru Erhan, Ian Goodfellow, and Rob Fergus. Intriguing Properties of Neural Networks. *arXiv preprint arXiv:1312.6199*, 2013.

Theano Development Team. Theano: A Python Framework for Fast Computation of Mathematical Expressions. *arXiv e-prints*, abs/1605.02688, May 2016.

Sergey Zagoruyko and Nikos Komodakis. Wide Residual Networks. *arXiv preprint arXiv:1605.07146*, 2016.

# Appendices

## A DERIVATION OF THE ACTIVATION HESSIAN RECURSION

Here, we provide the basic derivation of the factorisation of the diagonal blocks of the Hessian in Eq. 1 and the recursive formula for calculating $\mathcal{H}$ as presented in (Botev et al., 2017).

The Hessian of a neural network with parameters $\theta$ as defined in the main text has elements:

$$[H]_{ij} = \frac{\partial^2}{\partial\theta_i \partial\theta_j} E(\theta) \tag{10}$$

For a given layer $\lambda$, the gradient w.r.t. a weight $W^{\lambda}_{a,b}$ is:

$$\frac{\partial E}{\partial W^{\lambda}_{a,b}} = \sum_i \frac{\partial h^{\lambda}_i}{\partial W^{\lambda}_{a,b}} \frac{\partial E}{\partial h^{\lambda}_i} = a^{\lambda-1}_b \frac{\partial E}{\partial h^{\lambda}_a} \tag{11}$$

Keeping $\lambda$ fixed and differentiating again, we find that the per-sample Hessian of that layer is:

$$[H_\lambda]_{(a,b),(c,d)} \equiv \frac{\partial^2 E}{\partial W^{\lambda}_{a,b} \partial W^{\lambda}_{c,d}} = a^{\lambda-1}_b a^{\lambda-1}_d \left[\mathcal{H}_\lambda\right]_{a,c} \tag{12}$$

where

$$[\mathcal{H}_\lambda]_{a,b} = \frac{\partial^2 E}{\partial h^{\lambda}_a \partial h^{\lambda}_b} \tag{13}$$

is the pre-activation Hessian.

We can reexpress this in matrix notation as a Kronecker product as in Eq. 1:

$$H_\lambda = \frac{\partial^2 E}{\partial \operatorname{vec}(W_\lambda) \partial \operatorname{vec}(W_\lambda)} = \left(a_{\lambda-1} a^{\mathsf{T}}_{\lambda-1}\right) \otimes \mathcal{H}_\lambda \tag{14}$$

The pre-activation Hessian can be calculated recursively as:

$$\mathcal{H}_\lambda = B_\lambda W^{\mathsf{T}}_{\lambda+1} \mathcal{H}_{\lambda+1} W_{\lambda+1} B_\lambda + D_\lambda \tag{15}$$

where the diagonal matrices $B$ and $D$ are defined as:

$$B_\lambda = \operatorname{diag}\left(\mathbf{f}'_\lambda(h_\lambda)\right) \tag{16}$$

$$D_\lambda = \operatorname{diag}\left(\mathbf{f}''_\lambda(h_\lambda) \frac{\partial E}{\partial a_\lambda}\right) \tag{17}$$

$\mathbf{f}'$ and $\mathbf{f}''$ denote the first and second derivative of the transfer function. The recursion is initialised with the Hessian of the error w.r.t. the linear network outputs.

For further details and on how to calculate the diagonal blocks of the Gauss-Newton and Fisher matrix, we refer the reader to (Botev et al., 2017) and (Martens & Grosse, 2015).

## B MATRIX NORMAL DISTRIBUTION

The matrix normal distribution (Gupta & Nagar, 1999) is a multivariate distribution over an entire matrix of shape $n \times p$ rather than just a vector. In contrast to the multivariate normal distribution, it is parameterised by two p.s.d. covariance matrices, $U : n \times n$ and $V : p \times p$, which indicate the covariance of the rows and columns respectively. In addition it has a mean matrix $M : n \times p$.

A vectorised sample from a matrix normal distribution $X \sim \mathcal{MN}(M, U, V)$ corresponds to a sample from a normal distribution $\mathrm{vec}(X) \sim \mathcal{N}(\mathrm{vec}(M), U \otimes V)$. However, samples can be drawn more efficiently as $X = M + AZB$ with $Z \sim \mathcal{MN}(0, I, I)$, and $AA^\mathsf{T} = U$ and $B^\mathsf{T}B = V$. The sample $Z$ corresponds to a sample from a normal distribution of length $np$ that has been reshaped to a $n \times p$ matrix. This is more efficient in the sense that we only need to calculate two matrix-matrix products of small matrices, rather than a matrix-vector product with one big one.

## C APPROXIMATION OF THE EXPECTED ACTIVATION HESSIAN

While the square root of $\mathcal{Q}_\lambda$ is calculated during the forward pass on all layers, $\mathcal{H}$ requires an additional backward pass. Strictly speaking, it is not essential to approximate $\mathbb{E}[\mathcal{H}]$ for the Kronecker factored Laplace approximation, as in contrast to optimisation procedures the curvature only needs to be calculated once and is thus not time critical. For datasets of the scale of ImageNet and the networks used for such datasets, it would still be impractically slow to perform the calculation for every data point individually. Furthermore, as most datasets are augmented during training, e.g. random cropping or reflections of images, the curvature of the network can be estimated using the same augmentations, effectively increasing the size of the dataset by orders of magnitude. Thus, we make use of the minibatch approximation in our experiments — as we make use of data augmentation — in order to demonstrate its practical applicability.

We note that $\mathbb{E}[\mathcal{H}]$ can be calculated exactly by running KFRA (Botev et al., 2017) with a minibatch-size of one, and then averaging the results. KFAC (Martens & Grosse, 2015), in contrast, stochastically approximates the Fisher matrix, so even when run for every datapoint separately, it cannot calculate the curvature factor exactly.

In the following, we also show figures for the adversarial experiments in which we calculate the curvature per datapoint and without data augmentation:

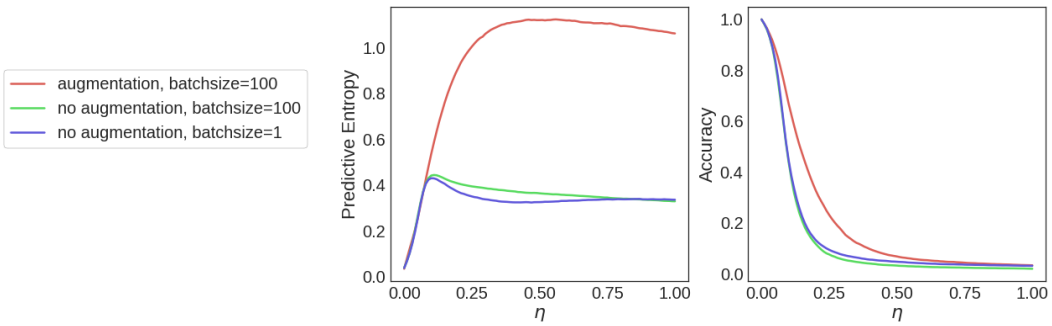


Figure 6: Untargeted adversarial attack for Kronecker factored Laplace approximation with the curvature calculated with and without data augmentation/approximating the activation Hessian.

Fig. 6 and Fig. 7 show how the Laplace approximation with the curvature estimated from 1000 randomly sampled binary MNIST images and the activation Hessian calculated with a minibatch size of 100 performs in comparison to the curvature factor being calculated without any data augmentation with a batch size of 100 or exactly. We note that without data augmentation we had to use much stronger regularisation of the curvature factors, in particular we had to add a non-negligible multiple of the identity to the factors, whereas with data augmentation it was only needed to ensure that the matrices are invertible. The Kronecker factored Laplace approximation reaches particularly high uncertainty on the untargeted adversarial attack and is most robust on the targeted attack when using data augmentation, suggesting that it is particularly well suited for large datasets and ones

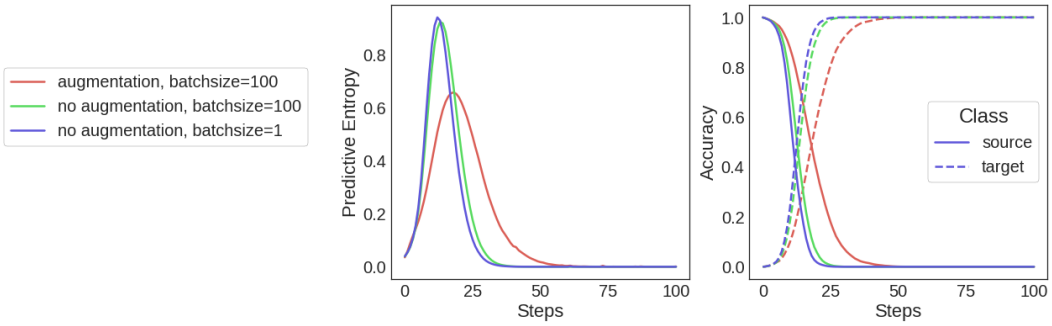


Figure 7: Targeted adversarial attack for Kronecker factored Laplace approximation with the curvature calculated with and without data augmentation/approximating the activation Hessian.

where some form of data augmentation can be applied. The difference between approximating the activation Hessian over a minibatch and calculating it exactly appears to be negligible.

## D Memory and Computational Requirements

If we denote the dimensionality of the input to layer $\lambda$ as $D_{\lambda-1}$ and its output as $D_\lambda$, the curvature factors correspond to the two precision matrices with $\frac{D_{\lambda-1}(D_{\lambda-1}+1)}{2}$ and $\frac{D_\lambda(D_\lambda+1)}{2}$ 'parameters' to estimate, since they are symmetric. So across a network, the number of curvature directions that we are estimating grows linearly in the number of layers and quadratically in the dimension of the layers, i.e. the number of columns of the weight matrices. The size of the full Hessian, on the other hand, grows quadratically in the number of layers and with the fourth power in the dimensionality of the layers (assuming they are all the same size).

Once the curvature factors are calculated, which only needs to be done once, we use their Cholesky decomposition to solve two triangular linear systems when sampling weights from the matrix normal distribution. We use the same weight samples for each minibatch, i.e. we do not sample a weight matrix per datapoint. This is for computational efficiency and does not change the expectation.

One possibility to save computation time would be to sample a fixed set of weight matrices from the approximate posterior — in order to avoid solving the linear system on every forward pass — and treat the networks that they define as an ensemble. The individual ensemble members can be evaluated in parallel and their outputs averaged, which can be done with a small overhead over evaluating a single network given sufficient compute resources. A further speed up can be achieved by distilling the predictive distributions of the Laplace network into a smaller, deterministic feedforward network as successfully demonstrated in (Balan et al., 2015) for posterior samples using HMC.

## E Prediction Accuracy

This section shows the accuracy values obtained from the different predictions methods on the feedforward networks for MNIST and the wide residual network for CIFAR100.

Table 1: Test accuracy of the feedforward network trained on MNIST

| Prediction Method | Accuracy |
|---|---|
| Deterministic | 98.86% |
| MC Dropout | 98.85% |
| Diagonal Laplace | 98.85% |
| **KF Laplace** | 98.80% |

In all cases, neither MC Dropout nor the Laplace approximation significantly change the classification accuracy of the network in comparison to a deterministic forward pass.

Table 2: Accuracy on the final $5,000$ CIFAR100 test images for a wide residual network trained with and without Dropout.

| | Accuracy | |
|---|---|---|
| Prediction Method | Dropout | Deterministic |
| Deterministic | 79.12% | 79.18% |
| MC Dropout | 79.20% | - |
| **KF Laplace** | 79.10% | 79.36% |

## F Implementation Details for Residual Networks

Our wide residual network has $n$=3 block repetitions and a width factor of $k$=8 on CIFAR100 with and without Dropout using hyperparameters as in (Zagoruyko & Komodakis, 2016). We only make one small modification to the architecture: instead of downsampling with $1\times1$ convolutions with stride 2, we use $2\times2$ convolutions. This is due to Theano not supporting the transformation of images into the patches extracted by a convolution for $1\times1$ convolutions with stride greater than $1$, which we require for our curvature backpropagation through convolutions.

We apply a standard Laplace approximation to the batch normalisation parameters — a Kronecker factorisation is not needed, since the parameters are one-dimensional. When calculating the curvature factors, we use the moving averages for the per-layer means and standard deviations obtained after training, in order to maintain independence between the data points in a minibatch.

We need to make a further approximation to the ones discussed in Section 2.2 when backpropagating the curvature for residual networks. The residual blocks compute a function of the form $res(x) = x + f_\phi(x)$, where $f_\phi$ typically is a sequence of convolutions, batch normalisation and elementwise nonlinearities. This means that we would need to pass back two curvature matrices, one for each summand. However, this would double the number of backpropagated matrices for each residual connection, hence the computation time/memory requirements would grow exponentially in the number of residual blocks. Therefore, we simply add the curvature matrices after each residual connection.